PNAS

# Supporting Information for

Differential nanoscale organization of excitatory synapses onto excitatory vs inhibitory neurons

Poorna A. Dharmasri, Aaron D. Levy, Thomas A. Blanpied

Thomas A. Blanpied
Email: TBlanpied@som.umaryland.edu

**This PDF file includes:**

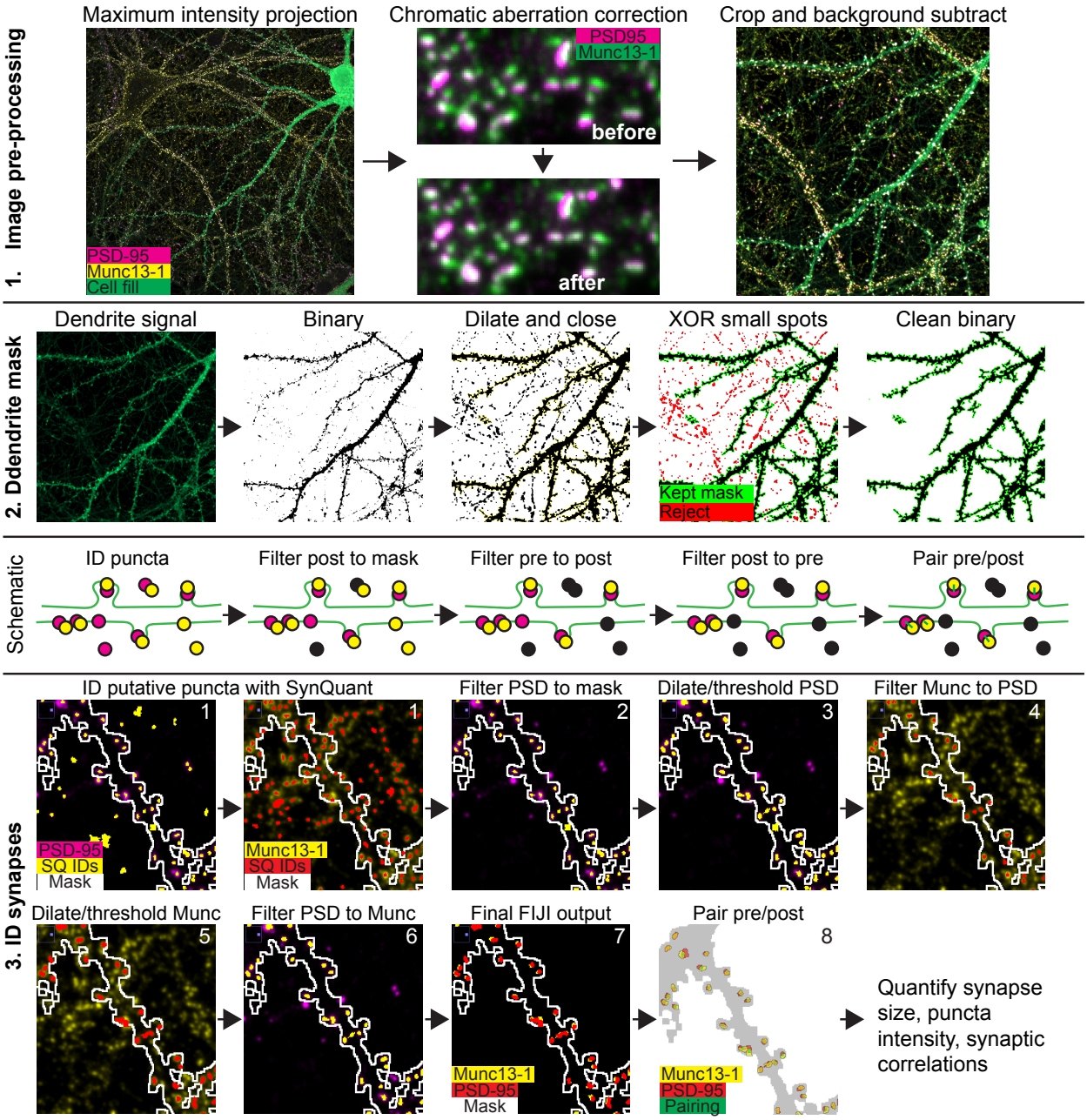


**Fig. S1.** Visual outline of image processing and quantification steps for confocal measurements in Figure 1.

Details are in Materials and Methods.

**1.** Images are pre-processed for analysis. Confocal z-stacks are maximum intensity projected, corrected for chromatic aberrations between channels, cropped to an area of interest, and background subtracted.

**2.** The dendrite mask is created to isolate synapses to the cell of interest. The dendrite signal is thresholded and binarized, and the binary adjusted. Small spots arising from off-cell background are selected then removed by an XOR operation against the entire selection, resulting in a clean binary.

**3 and schematic.** Synaptic puncta are identified on the cell of interest. Schematic shows which puncta are removed in each filtering step shown in 3; magenta are postsynaptic puncta and yellow

presynaptic. ROIs are identified by SynQuant in both channels. Then, postsynaptic ROIs are filtered to those that overlap with the dendrite mask and adjusted to the size of the actual puncta. Presynaptic ROIs are filtered to those that overlap with the postsynaptic ROIs, adjusted for size, and finally postsynaptic ROIs are filtered to those that overlap with the presynaptic ROIs, leaving a set of putative “synaptic” ROIs. ROIs are confirmed as synaptic if they have a mutually closest neighbor within a 500 nm maximum distance, then are quantified.

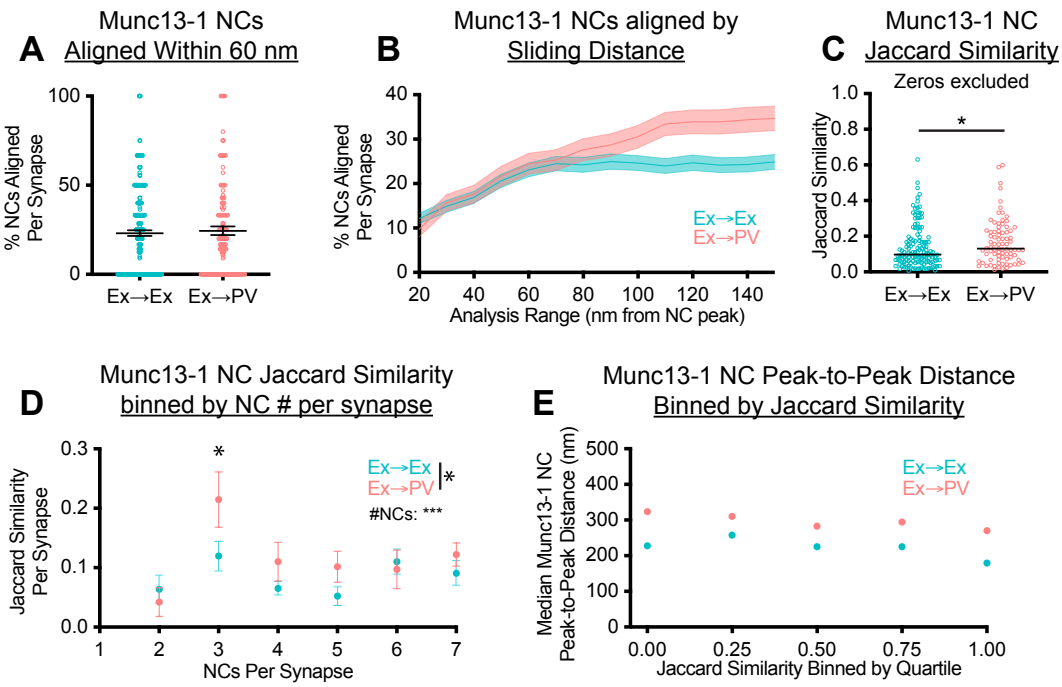


**Fig. S2.** Additional analyses of trans-synaptic organization and schematic related to Figure 4.

**A)** Both synapse types have equal proportions of Munc13-1 NCs aligned to PSD-95 within 60 nm of the NC peak (means ± SEM, Ex→Ex, 23.11 ± 1.57%, n = 237 synapses; Ex→PV 24.49 ± 2.35%, p = 0.7837, n = 124 synapses).
**B)** Both synapse types have an equal proportion of Munc13-1 NCs aligned to PSD-95 up to 100 nm away from the NC peak, after which they diverge.
**C)** High per-synapse nanocolumn diversity, as well as the difference between synapse types, remain when synapses lacking any nanocolumn similarity (i.e. with Jaccard similarity coefficient (JS) = 0) are removed from analysis (compare to Fig 4H where zeros are not removed) (median JS: Ex→Ex, 0.098, n = 132; Ex→PV, 0.13, n = 81; p = 0.037).
**D)** JS of Munc13-1 NC enrichment with PSD-95 subset by number of Munc13-1 NCs per synapse. While there are statistically significant main effects of NC number and synapse type (two-way ANOVA; NC number: p = 0.0005, synapse type: p = 0.0451), with 3 NC Ex→PV synapses having higher average JS than and Ex→Ex (post-hoc Šidák test; p = 0.0419), the effect of NC number is minimal with a mean difference <0.1 for 3 NC synapses and <0.05 for other groups (n for 2-7 NC groups (Ex→Ex/Ex→PV) = 34/13, 36/17, 41/18, 29/19, 25/13, 19/13 NCs).
**E)** Munc13-1 NCs are slightly farther apart in Ex→PV synapses than Ex→Ex synapses, but the median distance between NCs does not change for either group with increasing Jaccard Index (n as in H). Data in A are individual nanoclusters with lines at mean ± SEM. Data in B show a line connecting mean of each bin ± SEM shading. Data in C are mean ± SEM of per synapse JS binned by number of NCs per synapse. Data in D are medians of all Munc13-1 NC peak-to-peak distances binned by JS quartile.

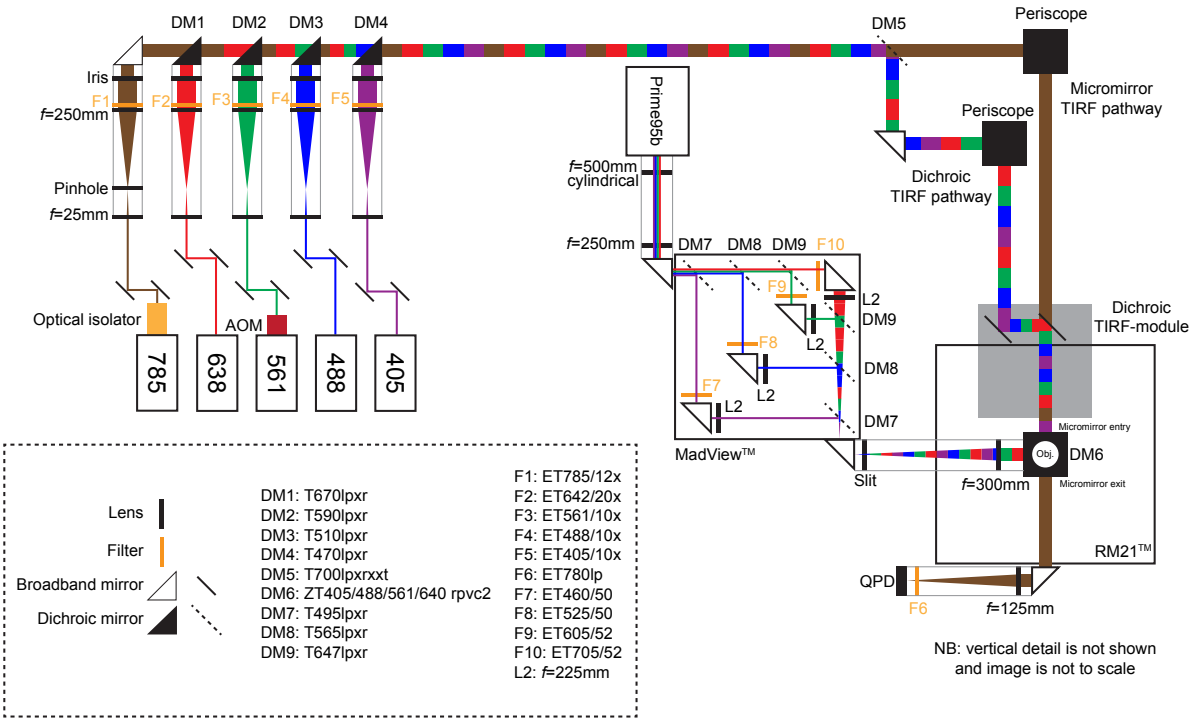


**Fig. S3.** Schematic of single-molecule microscope.

See SI Materials and Methods *Single-molecule microscopy* section for detailed description.

## Table S1: Primary antibodies

| Primary antibodies | Source | RRID | Stock concentration | Dilution |
|---|---|---|---|---|
| Polyclonal chicken anti-GFP | Thermo Fisher A10262 | AB_2534023 | 1 mg/mL | 1:500 |
| Guinea pig anti-parvalbumin antiserum | Swant GP72 | AB_2665495 | 1 mg/mL | 1:500 |
| Monoclonal mouse IgG2A anti-PSD95 (clone K28/43) | Neuromab 75-028 | AB_2877189 | 0.5 mg/mL | 1:80 |
| Polyclonal rabbit anti-Munc13 | Synaptic Systems 126103 | AB_887733 | 0.5 mg/mL | 1:250 |

## Table S2: Secondary antibodies

| Secondary reagents | Source | RRID | Stock concentration | Dilution |
|---|---|---|---|---|
| Donkey anti-chicken AlexaFluor488 | Jackson ImmunoResearch 703-545-155 | AB_2340375 | 1.25 mg/mL | 1:500 |
| Donkey anti-guinea pig AlexaFluor488 | Jackson ImmunoResearch 706-545-148 | AB_2340472 | 1.25 mg/mL | 1:500 |
| Goat anti-mouse IgG2a | Jackson ImmunoResearch 115-005-206 (conjugated to Cy3B in-house) | AB_2338462 | ~1.25 mg/mL | 1:500 |
| Donkey anti-rabbit AlexaFluor647 | Jackson ImmunoResearch 711-605-152 | AB_2492288 | 1.25 mg/mL | 1:500 |
| FluoTag-XM-QC anti-mouse IgG kappa light chain sdAb (clone 1A23) + docking site F1 | Massive Photonics (custom) | | 5 µM | n/a |
| FluoTag-XM-QC anti-rabbit IgG sdAb (clone 10E10) + docking site F3 | Massive Photonics (custom) | | 5 µM | n/a |
| ChromPure Rabbit IgG, Fc fragment | Jackson Immunoresearch 011-000-008 | | n/a | n/a |

## SI Materials and Methods

***DNA constructs:*** pFCaGW is a lentiviral vector that expresses EGFP (G) under the CaMKII promoter (Ca). The pCaMKII-EGFP transcriptional unit was assembled into a custom backbone (derived from (1), a gift from Alexandros Poulopoulos, and the pEGFP-N1 backbone (Clontech)) by Golden Gate Assembly (NEB), with the CaMKII promoter from mCh-GluA1-CIB (a gift from Matthew Kennedy (Addgene plasmid # 89444; http://n2t.net/addgene:89444; RRID:Addgene_89444)), and EGFP from pEGFP-N1. pCaMKII-EGFP was inserted by NEB HIFI Assembly into the PacI site of a modified pFUGW vector (pFW), where the ubiquitin promoter and EGFP were deleted by KLD mutagenesis (NEB), yielding pFCaGW. For all cloning reactions, fragments were generated by PCR with KAPA HiFi HotStart DNA polymerase (Roche) or by DNA synthesis (IDT), and correct clones were confirmed by whole plasmid sequencing using Oxford Nanopore Technology with custom analysis and annotation (Plasmidsaurus). psPAX2 (Addgene plasmid # 12260; http://n2t.net/addgene:12260; RRID:Addgene_12260) and pMD2.G (Addgene plasmid # 12259; http://n2t.net/addgene:12259; RRID:Addgene_12259) were gifts from Didier Trono.

***Lentivirus production:*** HEK293T cells (ATCC CRL-3216) were maintained in DMEM + 10% FBS and penicillin/streptomycin. To make lentivirus, 5 x $10^6$ cells were plated on a 10 cm dish, then transfected 24h later with 6 µg pFCaGW, 4 ug psPAX2, and 2 µg pMD2.G using PEI (1 µg DNA : 3 µg PEI) for 4-6h before replacing the HEK media with neuron culture media. The media was harvested 48h later, centrifuged at 1000 x g for 5 minutes and filtered through a 0.45 µm PES filter to remove debris, and stored at -80˚C in single-use aliquots. Titers were routinely in the $10^5$-$10^6$ IFU/mL range.

***Primary neuron culture:*** All animal procedures were approved by the University of Maryland Animal Use and Care committee. Dissociated primary hippocampal neuron cultures were prepared from E18 Sprague-Dawley rat embryos (Charles River) of both sexes. Hippocampus was isolated and dissociated with trypsin, and cells were plated on poly-L-lysine-coated coverslips at 30,000 cells/coverslip (18 mm #1.5, Warner Instruments) in Neurobasal A + GlutaMax, gentamycin, B27 supplement, and 5% FBS. After 24 hours, the media was changed to the same but lacking FBS, and after 1 week supplemented with an additional half volume media + FUDR to suppress glial growth. Neurons were infected at DIV5 with 50 µl of unconcentrated pFCaGW lentivirus and fixed at DIV21 for both confocal and DNA-PAINT experiments.

***Antibody-dye conjugation:*** 300 µl of donkey anti-mouse IgG2a was concentrated on a 100K MWCO Amicon spin filter (Sigma) and diluted to ~2.5 mg/mL with pH8.3 PBS, then mixed with NHS-Cy3B (GE) at ~13:1 molar ratio of dye:IgG for 1h at RT to achieve a final dye/IgG ratio of ~3:1. Excess dye was removed by Zeba 7K MWCO spin desalting column (Thermo Fisher), and the dye/protein ratio confirmed by absorbance at 559 nm and 280 nm according to the manufacturer's instructions. Conjugated antibody was diluted to ~1.25 mg/mL in 50% glycerol, aliquoted, and stored at -20˚C.

***Immunostaining:*** pFCaGW-infected and naïve coverslips from the same plate were fixed with 2% PFA + 4% sucrose in PBS for 10 minutes at room temperature (RT), washed 3 x 5 minutes with PBS + 100 mM glycine (PBSG), permeabilized 20 minutes RT with 0.3% Triton X-100 in PBSG, and blocked 1h RT with 10% donkey serum + 0.2% Triton X-100 in PBSG.

For confocal imaging, the neurons were stained overnight at 4˚C with primary antibodies mouse IgG2A anti-PSD-95, rabbit anti-Munc13-1, and chicken anti-GFP (for pFCaGW-infected cells) or guinea pig anti-PV (for naïve cells) in 5% donkey serum + 0.1% Triton X-100 in PBSG. The next day, cells were washed 3 x 5 minutes in PBSG, then incubated with the secondary antibodies goat anti-mouse IgG2a Cy3B, donkey anti-rabbit AlexaFluor647, and either donkey anti-chicken AlexaFluor488 (pFCaGW) or donkey anti-guinea pig AlexaFluor488 (naïve) for 1 hour at RT in

PBSG. Finally, the cells were washed 3 x 5 minutes PBSG, post-fixed with 4% PFA + 4% sucrose in PBS for 15 minutes, and washed 3 x 5 minutes PBSG again before storage at 4˚C until imaging.

For DNA-PAINT, PSD-95 and Munc13-1 were stained with primaries preincubated with custom-made single-domain antibodies (sdAbs; Massive Photonics) carrying one of two oligonucleotide docking strands optimized for DNA-PAINT, as described (2, 3). Briefly, the primary antibodies against PSD-95 and Munc13-1 were incubated separately with a 2.5-fold molar excess of anti-mouse sdAb-F1 or anti-rabbit sdAb-F3, respectively, for 20 minutes at RT, to saturate the antibody with sdAb. Rabbit Fc fragment was added to the Munc13-1 incubation at 2-fold molar excess for a further 20 minutes to remove unbound nanobody. Both preincubations were then diluted to their final working concentrations in 5% donkey serum + 0.1% Triton X-100 in PBSG, along with chicken anti-GFP or guinea pig-anti PV, and incubated on the cells overnight at 4˚C. The next day, the cells were processed as for confocal imaging, but including only the appropriate AlexaFluor488 secondary. 90 nm gold nanoparticles (Cytodiagnostics) were added at 1:10 dilution for 10 minutes before imaging as fiducials for drift and chromatic aberration correction. Antibody details can be found in Tables S1 and S2.

***Confocal microscopy:*** Confocal images were acquired on a Nikon TI2 Eclipse inverted microscope equipped with a piezo unit for Z control (ASI), a Nikon Apo TIRF 60x/1.49 NA objective and a Dragonfly confocal unit (Andor). Excitation laser light (488, 561, or 638 nm) from an Andor ILE, flattened by an Andor Beam Conditioning Unit, was passed to the sample by a 405/488/561/640 quadband polychroic (Chroma). Emission light was passed through an appropriate bandpass filter (ET525/50, ET600/50 (Chroma), or Em01-R442/647 (Semrock), for AlexaFluor488, Cy3B, and AlexaFluor647 emission, respectively) and collected on a Zyla 4.2 sCMOS camera (Andor). Cells of interest were imaged with 10 µm thick confocal z-stacks with 0.3 µm z-steps at 50% laser power (~1-2 W/cm$^2$) with 200 ms exposure, with each channel imaged sequentially. Reference bead stacks for chromatic aberration correction were acquired by immobilizing 100 nm TetraSpeck beads (Invitrogen) on a poly-L-lysine-coated coverslip and imaging z-stacks as above.

***Confocal analysis:*** Most confocal image processing was performed with custom macros in FIJI (4), and the processing steps are summarized in Figure S1. First, a reference translation mask for chromatic aberration correction was generated from the TetraSpeck bead stacks using the NanoJ Core (5) plugin *Register Channels – Estimate*, then experimental z-stacks were converted to maximum intensity projections and chromatic aberrations corrected using NanoJ Core *Register Channels – Apply.* Next, each image was cropped to clean areas of GFP or PV signal, background subtracted by the lowest 1% pixel value per channel, and the GFP or PV image manually thresholded to select dendrites. The dendrite masks were cleaned up in two steps. First, the binary was smoothed with *Process>Binary>Dilate* 2x followed by *Close Holes*, then, small background particles in the mask were identified by *Analyze>Analyze Particles* with a size limit of 0-10 pixels, and each identified spot was removed from the mask by an XOR operation against the entire selection. The binary image was cropped to the resulting ROI and used as the dendrite mask. Putative synaptic puncta were identified in each channel with permissive settings of the plugin SynQuant ((6) z-score 10, minfill 0.65, whratio 6, min size 10, max size 200), which in our dataset identified many real puncta but also some generally large background spots. These spots were refined through a series of filtering steps 1) postsynaptic ROIs were removed if they did not overlap with the dendrite mask; 2) as we found that SynQuant worked well to identify puncta but less well to identify puncta size in our dataset, the remaining postsynaptic ROIs were dilated by 2 pixels to encompass the entire puncta then thresholded to 40% of the maximum intensity within the ROI to better capture the entire puncta; 3) presynaptic ROIs were removed if they did not overlap with the postsynaptic puncta from step 2; 4) remaining presynaptic ROIs were dilated and thresholded as in step 2; 5) postsynaptic ROIs were removed if they did not overlap with the

presynaptic ROIs from step 4. PSD-95 and Munc13 puncta mean and integrated intensities as well as area were finally measured from the background-subtracted images in the remaining post- and pre-synaptic ROIs, respectively. Finally, pre and postsynaptic puncta were paired, using a custom script in MATLAB, by, for each PSD-95 ROI centroid, identifying the mutually closest Munc13 ROI centroid within a search radius of 500 nm. Outliers with area greater than 0.5 $\mu m^2$ were removed from the dataset as puncta larger than this were frequently visibly mis-segmented. Data were processed in R and intensities normalized to the mean of the Ex→Ex group, per week, to control for variance in staining and imaging across culture weeks.

***Single-molecule microscopy:*** 3D DNA-PAINT images were acquired on a custom microscope (Fig S3) built around an RM21 base (Mad City Labs), equipped with an infinity-corrected Olympus UPlanApo60x OHR/1.5 NA objective and stage piezo nanopositioner, as well as both micromirror and dichroic-based TIRF pathways. Excitation lasers (405, 488, 561, 638, and 785 nm; Oxxius) are separately expanded 10x by an *f*=25 mm asphere and *f*=250 mm achromatic doublet lens pair, cleaned up by a narrow bandpass filter, and cropped to 8 mm by an adjustable iris, then are combined into the same path by a series of longpass dichroics. The 785 nm laser additionally passed through an optical isolator before beam expansion, and a 25 µm pinhole just after the asphere to produce a higher quality beam for focus lock. To achieve focus lock, the 785 nm laser is passed through a T660lpxr dichroic and directed to the micromirror TIRF pathway of the RM21, which directs the beam to TIR and catches the exit beam on the far side of the objective. The exit beam is passed through a cleanup filter (ET780lp) and passed to a QPD such that deflections in the beam position due to focus shifts are compensated in a closed-loop system with the stage nanopositioner to maintain sample focus with high fidelity and responsiveness. The 405, 488, 561 and 638 nm lasers are reflected by the T660lpxr dichroic and directed to the dichroic TIRF module, which directs and focuses the beams off-center in the back aperture of the objective via a ZT405/488/561/640 rpvc2 quadband polychroic to achieve an adjustable illumination angle of the sample from epi to TIR. The micromirror and dichroic TIRF modules direct the laser to orthogonal positions on the objective back aperture for simultaneous imaging and focus lock. Emission light is focused by an *f*=300 mm achromatic doublet onto an adjustable rectangular iris, and is split in the MadView (MadCity Labs), in which a series of longpass dichroics reflect emission from 488, 561 and 640 excitation through separate adjustable *f*=225 mm lenses, allowing separate control of chromatic aberrations for each imaging channel. The emission lines are recombined by paired dichroics and focused onto a Prime 95b sCMOS camera (Photometrics) with an *f*=250 mm lens, first passing through an *f*=500 mm cylindrical lens to provide astigmatism for 3D imaging. The recombination of emission lines was done such that two-color simultaneous imaging was achieved by separating the parts of the camera chip receiving each color. The system achieves a final magnification of 110x, yielding a pixel size of 100 nm.

***Single-molecule imaging:*** GFP or PV-positive cells were identified with low power 488 nm laser. F1-Atto643 (for PSD-95) and F3-Cy3B (for Munc13) imagers were diluted in imaging buffer (1x PBS pH7.4 + 500 mM NaCl + PCA/PCD/Trolox oxygen scavengers; 59) to 0.25 nM each and added to the sample, which was allowed to equilibrate for at least 10 minutes to reduce drift. Then, 40,000 frames were acquired with 150 ms exposure, with laser power densities at the sample of 0.10 $kW/cm^2$ for the 638 nm laser and 0.059 $kW/cm^2$ for the 561 nm laser. The 785 nm laser was set to 50% power and used for focus lock. Imaging buffer was refreshed between regions.

***Single-molecule localization:*** Molecule locations were determined using the Super-resolution Microscopy Analysis Platform, SMAP (7). Z stacks of the 3D PSF of 100 nm TetraSpeck beads on coverglass were captured with 10 nm step size and a standard curve relating PSF characteristics to z position, from which z position of molecules was derived, was generated in SMAP using the *calibrate3DsplinePSF* plugin. Parameters were kept as default with the following exceptions: 1) the 3D modality was set as *global 2 channel* and *focus as z ref* was toggled to treat

the in-focus PSF as the 0 nm position in z; 2) *Global Fit Parameters* were modified to set *main Ch* as *u/l* and *right-left* with *Split (pix)* set to the distance in x in pixel units that bisected the image – this, in accordance with the simultaneous two-color imaging described above, ensures that the same beads formed the basis of each color's individual calibrations. Beads were selected on one side of the image using *Spatially resolved calibration: Interactive ROI, rectangular, right-left* with *no mirror*. To enable chromatic aberration correction and overlay of channels (see below), 5-10 regions of in-focus TetraSpeck beads were imaged without astigmatism for 100 frames and localized using SMAP. Images were loaded using *TifLoader*. *PeakFinder* settings were left at default and *PSF free* fitter was used with ROI size 7. For 3D experimental images, *PeakFinder* and *Fitter* settings were adjusted such that *DoG = 2.5*, *cutoff = 2*, *ROI size = 15*, and the *spline* fitter was used, adjusting the RI mismatch to 0.83 as appropriate for the system and loading the previously calculated 3D calibration.

***Single-molecule analysis:*** All analyses were performed with 3-dimensional data and conducted using custom routines in MATLAB (Mathworks) which relied, in part, on command line calls to Picasso (8) for specific functions.

*Processing of super-resolution images* - To correct chromatic aberrations between the channels, the localizations from the 2D bead images described above were first bisected and overlaid, followed by a nearest neighbor approach to match localized beads between the channels. A transformation matrix was subsequently generated using the *fitgeotrans* function in MATLAB with the input ('polynomial',2). This transformation was applied to the experimental data following cross-correlation-dependent drift correction, which was conducted using Picasso Render's *Undrift by RCC* function. The two channels were then more precisely aligned using a cross-correlation to align fiducial markers and then treated individually hereafter until noted otherwise. Poorly fit molecules were eliminated if their: localization precision was greater than 20 nm, PSF standard deviation was greater than 2 pixels, photon count was smaller than the mode of the whole-field histogram, or relative log likelihood was less than the first shoulder in the histogram (~-1.5). This resulted in a median xy localization precision for Munc13-1 of 2.35 nm in the Ex→Ex synapses and 2.54 nm in the Ex→PV synapses and a median xy localization precision for PSD-95 of 6.52 nm in the Ex→Ex synapses and 6.94 nm in the Ex→PV synapses. Localizations that persisted over multiple frames were merged using Picasso Render's *Link localizations* function, with max distance of 30 nm and max transient dark frames of 5. We noticed that the SMAP localization resulted in some molecules localized at an artificial extreme ceiling or floor in z, whose specific value depended on the calibration calculated in SMAP; these were eliminated from the analysis on a per image basis.

*Identifying putative synapses* - To automatically segment objects from the image, the Picasso Render *Clustering>DBSCAN* function was used with radius of 30 nm and minimum density of 5. Identified objects were filtered on the mean and standard deviation of the frames in which localizations within each object were present – this helped avoid inclusion of leftover gold fiducials (high standard deviation of frame number) or any clusters that were formed by nonspecific binding and localization of individual imager strands (low/high mean and low standard deviation of frame number). Clusters were further filtered by extracting PSD-95 clusters whose 2D projection overlapped with at least 1 localization of Munc13-1, using the *alphaShape* and *inShape* functions in MATLAB. The resultant clusters were then used to similarly filter the Munc13-1 clusters. Both protein species were then treated as if from the same population of molecules and were segmented into putative synapses using MATLAB's *dbscan* function with epsilon of 30 nm and minpts of 4. As a quality control measure, manual inspection of the resulting putative synapses enabled manual segmentation where DBSCAN had failed to separate two synaptic clusters. To filter down to the best sampled and well-segmented synapses, PSDs that contained fewer than 20 localizations, or whose long/short axis ratio was greater than 4, or whose area was less than

1.5 pixels or larger than 20 pixels were removed. The remaining putative synapses were then judged for quality based on sampling density, corresponding presence and shape between both Munc13-1 and PSD-95 clusters, and z spread of localizations. Synapses were sorted for cis- and/or trans-synaptic analyses based on these qualities and putative outlier localizations (which could impact synaptic volume and shape-based analyses) were removed by calculating the mean x, y, and z position of each point cloud and keeping only those localizations that fell within 2 standard deviations.

*Quantitative analysis of synaptic nanostructure* – Auto- and cross-correlation analyses were conducted as described previously (9). Nanocluster detection relied on the *dbscan* function in MATLAB, which after testing several cluster detection methods was most consistently able to identify Munc13-1 NCs in their heterogeneous distributions while also being easily modified with a factor to identify nanostructure in the relatively more homogenous PSD-95 distribution. The pairwise distance between each localization was computed and input to the *dbscan* function, along with an epsilon and minpts value that is unique to each point cloud, and the optional inputs ('Distance','precomputed'). Epsilon for each point cloud was determined first by calculating the mean minimal distance for each point within the point cloud and multiplying by an empirically determined factor that was specific to each protein species (30 random point clouds tested to determine most representative factor yielded 1.6 for Munc13-1 and 2.7 for PSD-95). Local density heat maps shown in Figures 2-4 were generated using the calculated epsilon for each synapse and thus represent the input to DBSCAN. The mean number of neighboring points within epsilon for each localization was calculated and minpts was set as 1.96 standard deviations above the result, rounded down. Synaptic and nanocluster volumes were calculated using either the entire synaptic point cloud or just the localizations assigned to a specific NC, respectively, by using the *volume* and *alphaShape* functions with an alpha radius of 150 nm. This radius was empirically derived as a radius at which the NC volume was minimally impacted by the addition or removal of edge points. While it may overestimate or "round" the NC shape relative to the tightest alpha radius, the use of just core points would underestimate the spatial extent of the NC, especially for Munc13-1 NCs, where a minimal alpha shape would be surrounded by points that would visually be apparent to be part of the NC. We therefore chose this more rounded alpha shape to avoid overemphasizing the noisier parts of detected NCs. The percentage of synaptic volume occupied by NCs was calculated by summing the individual volumes of each NC in each synapse and dividing by the overall volume of the matched synaptic compartment. Auto- and cross-enrichment analyses were calculated as described previously (9, 10), with one exception. The normalization in both analyses was conducted to a pseudorandom distribution of the same number of measured localizations whose only constraint was to guarantee one localization per bin – this was done to eliminate *NaN* and *Inf* outputs that would mask data in the real distribution due to 0s appearing in the randomized one. This strategy could result in individual bins that were normalized to a value of 1 having an outsized impact on the shape of the curve. To mitigate this possibility, the auto- and cross-enrichment curves were smoothed by first detecting outliers in each distance bin using a ROUT of 0.1% in PRISM (GraphPad), then calculating the maximum non-outlier value in each bin, and finally replacing the outlier values in each bin with the corresponding value. This maintains the influence of high-density regions on the curve but tempers inflation due to random chance. Prior to the cross-enrichment, the PSD-95 point cloud was shifted onto the Munc13-1 point cloud based on the cross-correlation of their shape, agnostic to any subsynaptic heterogeneity (9, 11). The percent of Munc13-1 NCs aligned with PSD-95 was calculated using the same base calculation of the cross enrichment, which yields a relative enrichment of the opposing protein within binned distances from the peak of a given NC. These values were averaged within a specific window. In parallel, a similar calculation was conducted on 50 random distributions of the opposing protein, bounded by the original cluster's shape and matching the original number of localizations. A NC was considered aligned if the average value was greater

than 1.96 standard deviations away from the mean of the random distributions. The range of the specific window depended on the analysis. In Fig S2A, it was within 60 nm of the peak. In Fig S2B, an iterative range was used in increments of 10 nm from 20-150 nm. In Fig 4G, a window of set width (30 nm) was used, but the binned distances used in the calculation were shifted within a range of 10-150 nm from the NC peak. A Jaccard similarity coefficient (JS) was calculated from the sliding window analysis in Fig 4G. First, the binned enrichment values, which take possible values of 1 if the NC was statistically enriched with PSD-95 at a given distance, 0 if the enrichment was statistically indistinguishable from that of a randomized PSD-95 point cloud, or -1 if the NC was statistically de-enriched, were binarized by combining 0s and -1s to 0s, thus creating a distance-ordered profile of 1s and 0s indicating PSD-95 enrichment for each Munc13-1 NC. The JS was then calculated for each pair of Munc13-1 NCs within a synapse as $JS(NC1, NC2) = \frac{a}{a+b+c}$, where *a* is the number of bins where both NC1 and NC2 are enriched with PSD-95, *b* is the number of bins where only NC1 is enriched and *c* is the number of bins where only NC2 is enriched. Therefore, the JS can range from 0 (no match between NCs at all/independent nanocolumn subtypes) and 1 (perfect match between NCs/identical nanocolumn subtypes). For example, a NC pair with enrichments of [1 1 1 0 0 0] and [1 0 1 1 1 0] has JS = 0.4, as 2 bins (1 and 3) have matching 1s, NC1 has 1 additional bin of enrichment, and NC2 has 2 additional bins of enrichment.

***Statistical analysis*** – Statistical analysis was conducted using GraphPad PRISM. Data were tested for normality using D'Agostino & Pearson, Shapiro-Wilk, and Kolmogorov-Smirnov tests. Data that passed normality checks were tested using two-tailed t-tests if variance was equal between groups or Welch's t-test if not, or with two-way ANOVA followed by post-hoc Šidák multiple comparison tests where appropriate. Data that did not pass these checks were tested with two-tailed Mann-Whitney tests. No statistical methods were used to predetermine sample size. Experimenters were blinded during super-resolution analyses.

**SI References**


1. R. R. Richardson, *et al.*, Enhancing Precision and Efficiency of Cas9-Mediated Knockin Through Combinatorial Fusions of DNA Repair Proteins. *CRISPR J.* **6**, 447–461 (2023).
2. S. Sograte-Idrissi, *et al.*, Circumvention of common labelling artefacts using secondary nanobodies. *Nanoscale* **12**, 10226–10239 (2020).
3. S. Strauss, R. Jungmann, Up to 100-fold speed-up and multiplexing in optimized DNA-PAINT. *Nat. Methods* **17**, 789–791 (2020).
4. J. Schindelin, *et al.*, Fiji - an Open Source platform for biological image analysis. *Nat. Methods* **9**, 10.1038/nmeth.2019 (2012).
5. R. F. Laine, *et al.*, NanoJ: a high-performance open-source super-resolution microscopy toolbox. *J. Phys. D* **52**, 163001 (2019).
6. Y. Wang, *et al.*, SynQuant: an automatic tool to quantify synapses from microscopy images. *Bioinforma. Oxf. Engl.* **36**, 1599–1606 (2020).
7. J. Ries, SMAP: a modular super-resolution microscopy analysis platform for SMLM data. *Nat. Methods* **17**, 870–872 (2020).
8. J. Schnitzbauer, M. T. Strauss, T. Schlichthaerle, F. Schueder, R. Jungmann, Super-resolution microscopy with DNA-PAINT. *Nat. Protoc.* **12**, 1198–1228 (2017).
9. A.-H. Tang, *et al.*, A trans-synaptic nanocolumn aligns neurotransmitter release to receptors. *Nature* **536**, 210 (2016).
10. A. M. Ramsey, *et al.*, Subsynaptic positioning of AMPARs by LRRTM2 controls synaptic strength. *Sci. Adv.* **7**, eabf3126 (2021).
11. J.-H. Chen, T. A. Blanpied, A.-H. Tang, Quantifcation of Trans-synaptic Protein Alignment: A Data Analysis Case for Single-molecule Localization Microscopy. *Methods San Diego Calif* **174**, 72–80 (2020).